Comprehensive Protection of Windings and Bearings for ASD Fed Motors

Copyright Material IEEE
Paper No. PCIC-(do not insert number)

John Houdek
Life Senior Member - IEEE
Allied Industrial Marketing, Inc.
W67N222 Evergreen Boulevard
Cedarburg, WI 53012 USA
jahoudek@alliedindustrialmarketing.com

Nitin Kulkarni
Helwig Carbon Products
8900 W Tower Ave
Milwaukee, WI 53224
USA
nitin.kulkarni@helwigcarbon.com

Randy Herche
Helwig Carbon Products
8900 W Tower Ave
Milwaukee, WI 53224
USA
randy.herche@helwigcarbon.com

Abstract – AC induction motors controlled by Adjustable Speed Drives (ASD) may be subject to power quality disturbances associated with Pulse Width Modulated (PWM) voltage which can adversely affect the electrical and mechanical life of the motor. PWM pulses can be reflected at the motor end of the cable and increase the peak voltage at the motor terminals. Excessive peak voltage due to voltage reflection, which is exacerbated by cable length and fast IGBT pulse rise times, can cause premature electrical failures in motor windings. Voltage rise, (*dv/dt*) associated with IGBT pulse rise time can also develop shaft voltage that ultimately causes discharge currents to flow through the bearings, leading to premature bearing failure. While these problems can exist in any motor application, they tend to be more pronounced in submersible pumping due to cable length and the high capacitance associated with underground cables. This paper explains multiple effects of PWM voltage on motors and demonstrates a comprehensive approach for protecting both the windings and bearings of ASD fed motors.

Index Terms — Adjustable Speed Drive (ASD), Common-Mode (CM), Differential Mode (DM), Variable Frequency Drive (VFD), Pulse Width Modulation (PWM), Reflected voltage, Pulse rise time, dv/dt, Sine-wave filter, Motor bearing current, Shaft voltage, Bearing protection, Shaft grounding brush, Stator-neutral-to ground voltage (V_{sng}), Shaft voltage (V_{sh}).

I. INTRODUCTION

Approximately two-thirds of electric motors in use today are in applications that could benefit from control by Adjustable Speed Drives (ASD) [1]. Many previous publications have explained the possible adverse effects of PWM inverters on some motor applications because most commercially available motors have been designed for operation on sine-wave power [2]. It has been noted that some motors fed by ASD PWM voltage have experienced premature winding failures due to excessive peak voltage caused by voltage reflection. Elevated motor temperature associated with ASD PWM voltage can also reduce service life.

For high-frequency Pulse Width Modulated (PWM) inverter fed induction motors, the primary cause of premature motor bearing failures is bearing currents [3], [4]. Articles also pointed out that bearing life may be reduced by electrical discharge machining (EDM) of the bearings due to shaft voltage and associated bearing discharge currents [3], [4]. These bearing currents are caused by common-mode voltage [4], [5], inherent in all PWM inverters, and the parasitic capacitances of the motor stator winding, rotor and bearings [5], [6]. The bearing failure mode can be experienced in various ways, such as fluting, frosting or etching of ball bearings and inner bearing races, as shown in Fig. 1.

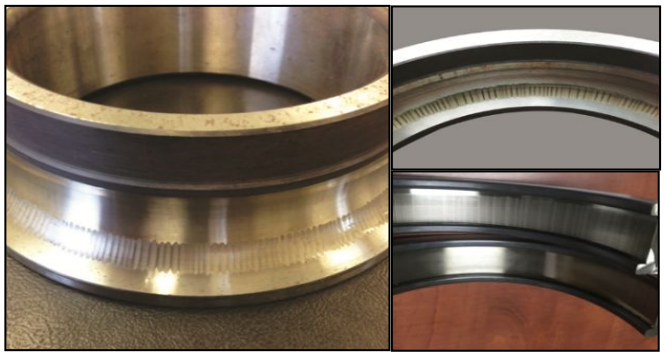

Fig. 1 Examples of Bearing Failures on ASD Fed Motors

The purpose of this paper is to study these common failure modes for ASD PWM fed motors by using computer simulation combined with actual testing of ASD fed motors. In addition, this paper examines the topics of voltage reflection and bearing erosion and quantifies the effects of sine-wave filters and shaft grounding brushes both individually as well as in combination with each other. Finally, the paper demonstrates a comprehensive approach for protecting motor windings and bearings against these adverse effects of ASD PWM voltage.

II. EFFECTS OF PWM ON ASD FED MOTORS

A. ASD PWM Output Waveform Characteristics

ASDs produce line-to-line (L-L) and line-to-neutral (L-N) voltage constructed from a series of square wave pulses, having varying widths depending on their location within the periodic cycle. This technique is known as pulse width modulation (PWM). The pulses have a height that is equal to the DC bus voltage. The number of pulses per half cycle is a function of the PWM inverter switching frequency. Although PWM voltage appears highly distorted, it can simulate the effect of sine-wave voltage and since motors have high inductance, the ASD output/motor current waveform is nearly sinusoidal. Fig. 2a illustrates typical ASD output voltage based upon computer simulation.

/20/$31.00 © 2022 IEEE

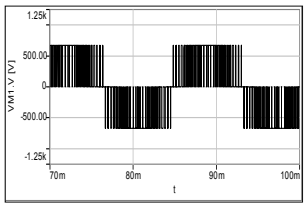

Fig.2a ASD output voltage

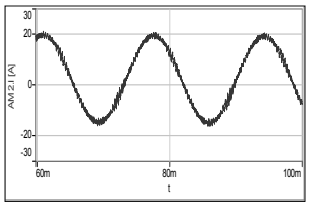

Fig.2b ASD fed Motor current

Fig. 2b shows the current for a ASD fed motor based upon computer simulation. In this scenario, the motor harmonic current distortion is 6.89% THD-i. The distortion is attributed primarily to harmonics of the inverter switching frequency (f_{sw}) which can increase the operating temperature of a motor in comparison to operation on sine-wave voltage and current [2], [7]. Motors controlled by ASDs can be expected to respond differently to the applied PWM voltage than they do when operating from pure sine-wave voltage.

B. Effects of PWM voltage on motor temperature

Current flowing in a motor at any frequency above its rated frequency will increase motor temperature rise. In the case of ASD-controlled motors, there is generally a small amount of low order harmonics plus harmonics associated with the PWM switching frequency (f_{sw}). As seen in Fig. 2b, the motor current contains a high-frequency ripple which is a combination of the PWM switching frequency current and several harmonics of this frequency. These high-frequency currents are responsible for increasing both the winding and iron losses in the motor [2], [7], [8]. Typically, the switching frequency has the most significant impact, but the 2nd through 5th harmonics (of f_{sw}) may also be relevant.

Due to the high-frequency currents flowing in motors fed from PWM voltage, these motors tend to experience higher temperature rise than the same motor when supplied from sinusoidal voltage. A comparison of motor temperature rise was reported for ASD fed motors [2], [7], [8]. For motors evaluated by the authors of [2] and [7], the motor temperature increased by as much as 4°C (10 hp) and 11°C (50 hp). Electrical insulation experiences accelerated aging when operating at elevated temperatures. A 10°C increase in operating temperature can generally result in a 50% reduction of motor insulation system life [8], [9].

Tables I and II illustrate test results [2] comparing the temperature rise for internal fan-cooled motors (10 hp and 50 hp) for operation on sine-wave voltage vs. PWM voltage. Elevated operating temperatures can weaken the dielectric strength of motor insulation systems and lead to shorter lifetimes. The temperature increase can be most significant for fan-cooled motors running at reduced speed since the fan will have less cooling effect at low speed.

TABLE I – 10 HP, 460 V MOTOR TEMPERATURE RISE [2]

Voltage	Hz	Speed	Torque	Amps (RMS)	Temp Rise
Sine	60	100%	100%	12.0	51°C
PWM	60	100%	100%	12.5	55°C
PWM	15	25%	87%	12.0	79°C
PWM	6	10%	89%	12.5	109°C

TABLE II – 50 HP, 460 V MOTOR TEMPERATURE RISE [2]

Voltage	Hz	Speed	Torque	Amps (RMS)	Temp Rise
Sine	60	100%	100%	59.1	62°C
PWM	60	100%	100%	61.4	73°C
PWM	30	50%	82%	56.8	72°C
PWM	6	10%	70%	51.3	94°C

NEMA standard MG-1 [10], Part 30.1.2 offers a motor derating curve (Fig. 3) for motors supplied from distorted voltage. Derating is based upon the harmonic voltage factor (HVF).

Harmonic voltage factor (HVF) is:

$$HVF = \sqrt{\sum_{n=5}^{n=\infty} \frac{V_n^2}{n}} \quad (1)$$

n = order of odd harmonic, excluding those divisible by three
V_n = p.u. magnitude of voltage at the n^{th} harmonic frequency

The distorted voltage will drive harmonic current into a motor at each frequency present, causing a higher temperature rise. Switching frequency harmonics can result in a higher harmonic voltage factor and therefore, some PWM-controlled motors will benefit from derating.

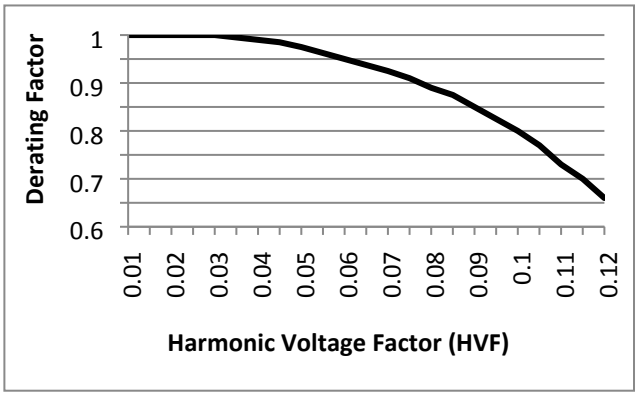

Fig. 3 Derating Curve per NEMA MG-1 Figure 30-1

C. Effects of dv/dt and voltage reflection on motors

The ASD peak AC output voltage is equal to the DC bus voltage, typically about 1.35 to 1.414 times the AC input voltage (L-L). For example, a 480 V drive has DC bus voltage of about 650 V_{dc} to 680 V_{dc} and therefore the peak AC voltage will be 650 V_{pk} to 680 V_{pk}.

Modern IGBT inverters have voltage pulse rise times in the range of about 50 *n*s to 400 *n*s [5], [8], [11], [12], which can result in *dv/dt* at the output terminals in the range of 1,700 to 14, 000 V/μs. Fast-rising pulses have high *dv/dt* rates and can be stressful on motor insulation systems, especially magnet wire insulation. Over-stressed insulation may experience accelerated aging resulting in premature dielectric breakdown.

For any motor cable length, a percentage of each voltage pulse will be reflected at the end of the cable and become additive to the original pulse, resulting in higher peak voltage at the motor than at the ASD. Voltage reflection is due to the mismatch between cable and load impedance values [8], [11], [12], [13]. Many ASD applications, especially submersible

/20/$31.00 © 2022 IEEE

pumping and some fan installations involve long motor cable lengths. As motor cable length increases, the peak voltage measured at the motor terminals increases up to a theoretical factor of two times the DC bus voltage (voltage doubling). In some cases, where the previous cable transient has not fully decayed before the next pulse reaches the end of the cable, it is possible to reach 3 p.u. over-voltage [11], [12].

Voltage doubling is expected for cables that exceed a critical cable length (l_{cr}) defined as:

$$l_{cr} = \frac{v \cdot t_r}{2} \quad (2)$$

Where: t_r = pulse rise time (μs)
v = pulse velocity on cable (about 150 m/μs)

Computer simulation demonstrates the voltage at the output of a 10 hp, 460 V, 60 Hz, (3 kHz switching frequency) ASD (Fig. 4a) and the motor (Fig. 4b) with 26 meters of XLPE cable between them. In this scenario, motor voltage has a peak value of 1,193 V, representing a reflected pulse of about 78% of the original pulse value (670 V).

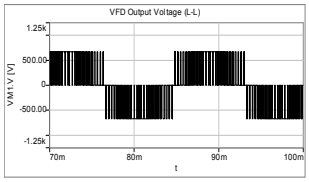

Fig. 4a voltage at ASD terminals

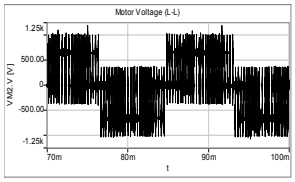

Fig. 4b voltage at motor terminals

Reflected pulses increase the peak voltage and *dv/dt* at the motor terminals, adding stress to the motor winding insulation, especially when already compromised by higher operating temperature. Articles [6], [13], [14] explain that a fast rise time pulse does not distribute equally over the motor winding. For a pulse with a rise time of 100 *n*s, up to 85% of the peak voltage will be "dropped" over the first turn of the first coil [6], [13], [14]. This explains why motor failure due to voltage reflection is often observed as a winding failure (short circuit) occurring within the first turn of the motor winding.

NEMA MG-1 [10], part 30 provides guidance for voltage stress by defining limits for peak voltage and pulse rise time, which also defines a *dv/dt* limit. In addition, the standard provides limits for voltage characteristics that motors should be able to withstand. NEMA std MG-1 [10], Part 30, Table III defines limits for "non-inverter duty" motors.

TABLE III – NEMA STD MG-1, PART 30 VOLTAGE LIMITS [10]

Motor Parameter	V_{rated} ≤600 volts	V_{rated} >600 volts
Peak voltage	≤ 1000 volts	≤ 2.04 x V_{rated}
Rise time	≥ 2 μs	≥ 1 μs

Low voltage motors conforming to NEMA standard MG-1 [10], Part 30 (non-inverter duty motors) should handle up to 1,000 V_{pk} and voltage rise times of 2 μs or slower. This also equates to a *dv/dt* limit of 500 V/μs. Motors rated 208-575 V have the same insulation capabilities and voltage limits. Therefore, motors of lower voltage ratings can typically handle a higher percentage of peak over-voltage.

NEMA std MG-1 [10], part 31, Table IV provides peak voltage and rise time limits for inverter duty motors. These limits apply to typical inverter duty motors, but not every "inverter duty" motor can withstand these limits. Motor manufacturers may interpret "inverter duty" as something besides the voltage and rise time limits per MG-1 [10], part 31. Some inverter duty motors may use the same dielectric insulation system as standard AC 60 Hz motors [12]. It is best to refer to the motor manufacturer for actual motor capabilities.

TABLE IV – NEMA STD MG-1, PART 31 VOLTAGE LIMITS [8]

Motor Parameter	V_{rated} ≤ 600 volts	V_{rated} > 600 volts
Peak voltage	≤ 3.10 x V_{rated}	≤ 2.04 x V_{rated}
Rise time	≥ 0.1 μs	≥ 1 μs

NEMA ICS 7.2-2015 [15] offers several techniques that can help to avoid detrimental effects of excessive peak voltages:

1) Use inverter duty motor per NEMA MG1, pt 31
2) Use a lower supply voltage (i.e.: 230 V ASD/motor)
3) Run the PWM control at the lowest carrier frequency
4) Avoid running multiple motors from a single ASD
5) Use a motor designed for V_{pk} = 3.1 x V_{rms}
6) Use a reactor or filter between drive and motor

Whether motors are inverter duty or not, PWM voltage waveforms can increase power losses and temperature rise. Typical motors can potentially operate with lower temperature rise and maximum service life when supplied from sine-wave voltage [2], [8]. Likewise, ASD fed motors will typically exhibit longer service life if the PWM pulsed voltage is converted to sine-wave voltage [8].

D. Effects of PWM pulsed voltage on bearings

PWM inverters produce common-mode voltage, which is the cause of motor bearing voltage, common-mode current and bearing discharge current [4], [6], [16], [17], [19]. Common-mode voltage results due to the fact the three ASD output phase voltages do not sum to zero. The asymmetry is visible in Fig. 5, where the three L-N voltages are displayed using computer simulation.

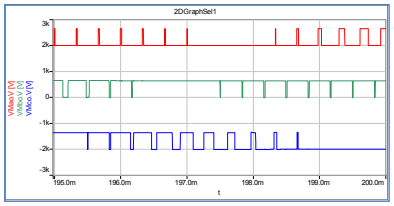

Fig. 5 L-N voltages for ASD output

The common-mode voltage is measured from the wye center point of the stator windings to frame ground. The (peak) common-mode voltage (V_{sng}) is equal to the $V_{dc\text{-}bus}$/2, except that for cable lengths exceeding the critical cable length (l_{cr}) there can also be voltage pulse reflections that increase this value [5], [9], [22]. For an ASD with 650 $V_{dc\text{-}bus}$ and 2-level inverter output, V_{sng} is expected to be about 325 V peak. This common-mode voltage (and resulting common-mode current) has a frequency equal to the PWM switching frequency [4], [18]. A portion of this voltage will also appear between the motor

/20/$31.00 © 2022 IEEE

shaft and motor frame (ground).

Fig. 6a illustrates V_{sng} for a 10 hp 460 V motor based upon computer simulation. The peak voltage is 325 V. Fig. 6b shows V_{sng} for a moderate cable length (26 m) which includes pulse reflections. In this case, V_{sng} is nearly 400 V peak. Voltage reflection, due to cable length, is responsible for increases to the L-L, L-N and V_{sng} voltages.

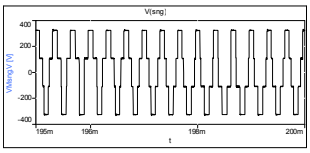

Fig. 6a V_{sng}

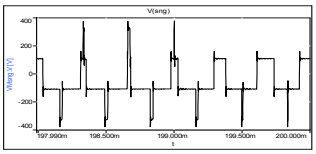

Fig. 6b V_{sng} with reflection

Applications using voltage source inverters experience high frequency (pulse transitions can be several megahertz) square wave voltage pulses with respect to the motor ground [16]. At these high frequencies, capacitively coupled currents can flow through paths typically considered insulators [16]. In addition, when motor cables are long, voltage reflection will cause the common-mode voltage (V_{sng}) to be higher than ½ $V_{dc\text{-}bus}$, potentially doubling to full DC bus voltage [5].

Common mode voltage (V_{sng}) affects bearing voltage through parasitic capacitances in the motor. At high frequencies, the motor has conductive parts insulated from each other, represented as parasitic capacitances [16], [18]. These high frequency capacitances, shown in Fig. 7a, consist of: stator to frame capacitance (C_{sf}), stator to rotor capacitance (C_{sr}), rotor to frame capacitance (C_{rf}) and bearing capacitance (C_b) [4], [5], [6], [9], [14], [15], [17 thru 27].

Common-mode voltage causes common-mode current to flow through the parasitic capacitances in the motor. A small portion of this common-mode current will flow from the windings through parasitic capacitances to the rotor and will ultimately flow through the bearings as it finds its way back to the grounded motor frame [17].

Bearing currents resulting from asymmetries in motor construction can also circulate through a closed-loop formed by the motor stator case, rotor shaft, and end bearings. These circulating currents may result from either inductive or capacitive coupling [21]. Other, non-circulating (discharge) currents [4], [5], [9], [16 thru 27] are caused by high *dv/dt* and parasitic capacitances (Fig. 7a and 7b). They flow through the rotor (shaft) to the motor frame (ground) through the bearings. These (discharge) currents are the most harmful as they can cause electrical discharge machining (EDM) in the bearings.

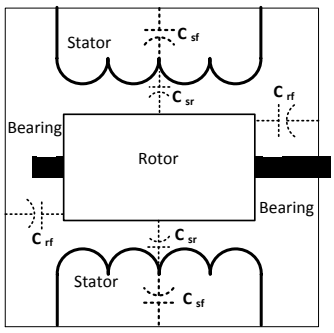

Fig. 7a parasitic capacitances

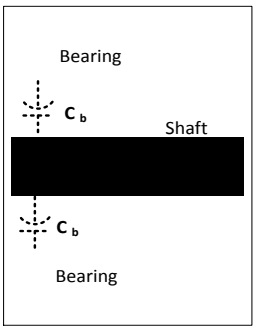

Fig. 7b Motor bearing capacitance

Bearing capacitance is depicted in the exploded view of the bearing circuit in Fig. 7b. The motor frame is ultimately grounded, providing the return path for these currents.

The bearing system consists of a lubricant (insulator) between two conductors (races, balls, rollers), forming a capacitor. According to [5], [9], [17], [19], V_{sng} and C_{sr} charge the high resistivity oil film that forms C_b. The typical dielectric strength of this lubricant is about 15 V_{pk}/µm of oil film and bearings have about 0.2 to 2.0 µm of oil film [5], [9], [22], [24]. Therefore, the breakdown voltage may be in the range of 3 to 30 V_{pk} [5], [9], [22], [24]. The thickness of the lubricant will vary with speed and temperature, altering the capacitance between shaft and bearing during motor operation [9], [23], [25].

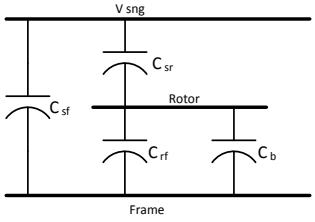

Fig. 8 Voltage divider circuit for parasitic capacitances

As can be seen in Fig. 8, bearing capacitance (C_b) is in parallel with the rotor to frame capacitance (C_{rf}) and these parallel capacitances are in series with the stator to rotor capacitance (C_{sr}). The shaft is part of the rotor; therefore, shaft voltage (V_{rg} or V_b) is determined by the voltage divider created by C_{sr} in series with the parallel (//) connection of C_{rf} and C_b. Bearing voltage (V_b) is measured from shaft to frame and will be less than but proportional to the common-mode voltage (V_{sng}). Voltage reflection, due to *dv/dt* and the cable length, can increase both V_{sng} and V_b.

As electric charge accumulates on the shaft, the voltage will increase until the lubricant breakdown voltage is reached. Then, a breakdown occurs and a discharge current flows into the bearing. There will be a discharge and a return to near-zero voltage followed by another accumulation of charges on the shaft and discharge in a high-frequency repetitive process [5], [9], [17], [19], [21], [22]. The shaft voltage (V_b or V_{rg}) can be calculated as follows:

$$V_{rg} = V_{sng} \times \frac{X_{c-rf}//X_{c-b}}{X_{c-sr} + (X_{c-rf}//X_{c-b})} \quad (3)$$

Where: $X_C = \frac{1}{2\pi f C}$

Based upon multiple sources [4], [20], [21], [22], [23], [24], [26

/20/$31.00 © 2022 IEEE

thru 30], typical values for parasitic capacitances for low voltage motors are shown in Table V. Bearing capacitance varies by motor size and rating, lubricant type, bearing type and motor operating conditions such as speed and load.

TABLE V TYPICAL MOTOR PARASITIC CAPACITANCES

Capacitor	Capacitance
C_{sf}	5-10 *n*F
C_{sr}	10-50 *p*F
C_{rf}	1-5 *n*F
C_b.	5 *p*F – 100 *n*F

The relationship between V_{sng} and V_b (V_{rg}) is a function of the parasitic capacitances and is defined by others [5], [9], [20], [21] as Bearing Voltage Ratio (BVR), where

$$BVR = \frac{C_{sr}}{C_{sr} + C_{rf} + C_b} = \frac{V_{rg}}{V_{sng}} \quad (4)$$

The BVR for the typical motor is about 0.10 [9], indicating that the shaft to ground voltage (V_b) will be about 10% of the common-mode voltage (V_{sng}). Since the contact area of the bearing is extremely small, the current density for any discharge can be substantial. Therefore, it does not take much shaft voltage to cause damage to motor bearings. Fig. 9 illustrates typical bearing voltage.

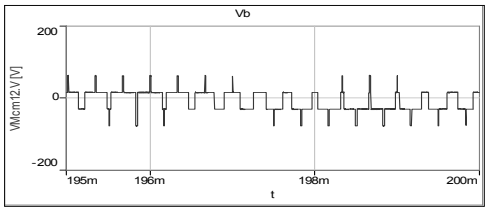

Fig. 9 Bearing Voltage (computer simulation)

Multiple sources [5], [10], [23], [31] suggest shaft voltage limits ranging from 0.3V to 1.414 V_{pk}. EPRI [31] in 2007 stated that "most induction motors are designed to have a maximum shaft voltage to frame ground of <1 V_{rms} (1.414 V_{pk})".

III. BASELINE MEASUREMENTS

A. Measurements for 10 hp, 460 V ASD fed motor (f_{sw}=3 kHz)

To verify the issues explained above, tests were conducted using a 10 hp ASD and motor with 26 m of motor cable (XLPE). Shaft voltage measurements were made using a low impedance, silver-graphite shaft grounding brush mounted on an insulator to the motor end bell face (Fig. 10a). The silver-graphite brush provides a sliding contact with extremely low resistance (Fig. 10b), suitable for measuring high-frequency shaft voltage [32]. The contact force must be low enough to avoid excess abrasive wear on a moving surface (shaft) but must be high enough for proper electrical contact [32]. The silver-graphite brush offers a compromise between mechanical and electrical factors. Fig. 10 illustrates the ideal range for pressure as it applies to sliding electrical contacts.

Fig. 10a Shaft Grounding Brush

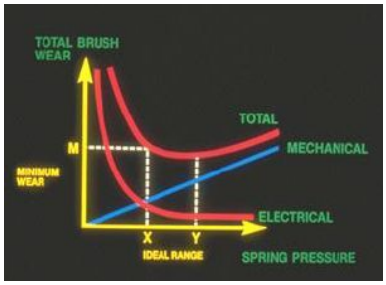

Fig. 10b Sliding Contact Pressure [32]

An oscilloscope was used to measure voltages and currents in the 460 V, 10 hp ASD fed motor system (Fig. 11). The time scales are varied according to the information sought. For example, when viewing 60 Hz fundamental waveforms, a time scale of 2 or 5 *m*s/div is used, whereas high-frequency data is obtained using faster scales of 200 µs, 100 µs and even 5 µs/div.

Baseline Measurements: 460V, 10 hp ASD + Motor (2 *m*s/div)		
Channel	**Parameter**	**Measurement**
CH 1 (blue)	Motor current	8.318 A_{rms}
CH 2 (red)	C-M current	159.6 mA_{rms} / 1.905 A_{pk}
CH3 (green)	Motor L-L Voltage	1,109 V_{pk}
CH 4 (pink)	Shaft Voltage	3.008 V_{rms} / 16.20 V_{pk}

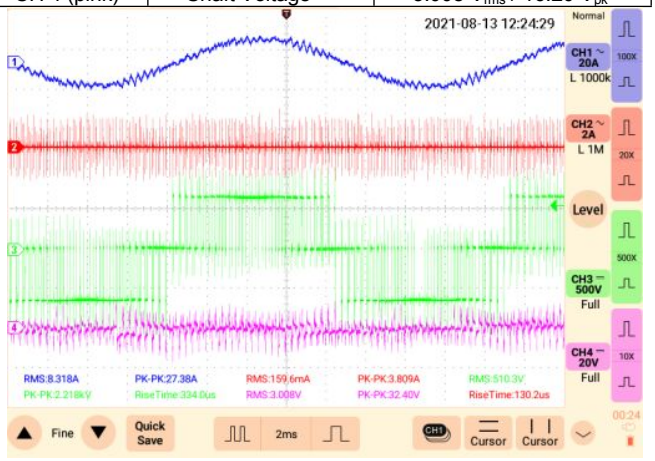

Fig. 11 (460 V, 10 hp) Baseline Motor Voltage and Current

Observations: motor current is sinusoidal with ripple at f_{sw}; Common-mode peak current is about 12 times the RMS value; Reflected voltage pulses increase the peak voltage about 70% higher than $V_{dc\text{-}bus}$ and V_{pk} (1,109 V) is above the NEMA MG-1, pt 30 limit; Shaft voltage is above the EPRI [31] suggested limit and high enough to cause bearing discharge currents.

These baseline measurements illustrate excessive motor peak voltage due to reflection, common-mode current and shaft voltage high enough to cause bearing discharges.

Common-mode current is a function of V_{sng} and common-mode impedance. The parasitic capacitances in the motor will charge and discharge with each voltage pulse causing impulses of common-mode current. A momentary short circuit occurs when the shaft voltage exceeds the dielectric strength of the lubricant and discharge current flows through the bearing to

/20/$31.00 © 2022 IEEE

ground. Therefore, bearing discharge currents can be viewed in the common-mode current as an impulse occurring when shaft voltage simultaneously goes to zero.

To measure common-mode voltage (V_{sng}), a 230 V, 5 hp motor (26 m cable) with a wye-connected stator winding was used. Using 30 Hz output helps maintain similar impedance for later tests involving the addition of a filter. Fig. 12 illustrates the measurement of V_{sng} versus the shaft voltage. The waveforms in Fig. 12 confirm that shaft voltage is similar in shape to the stator neutral to ground voltage (V_{sng}) but is proportionately and significantly lower based upon the capacitive voltage divider.

230 V, 5 hp V_{sng} and Shaft Voltage (200 µs)		
CH 3 (green)	V_{sng}	266.6 V_{pk}
CH 4 (pink)	Shaft voltage	4.854 V_{rms} / 9.86 V_{pk}

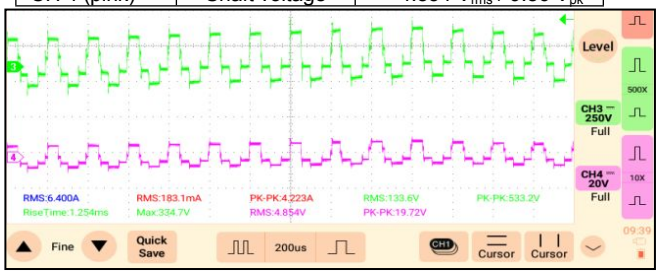

Fig. 12. (230 V, 5 hp) measurements of V_{sng} and shaft voltage

Observations: V_{sng} (250 V per division) is considerably higher than its expected value of 162.5 V_{pk} due to voltage reflection associated with this 26 m cable length; Shaft voltage (20 V per division) is similar in appearance to V_{sng} but considerably lower in amplitude.

IV. EVALUATION OF MOTOR PROTECTION METHODS (FILTER AND SHAFT GROUNDING BRUSHES)

A. Sine-wave filter

The traditional method to improve the L-L voltage waveform, reduce *dv/dt* and eliminate voltage reflection is to add a sine-wave filter (Fig. 13a) at the ASD output. These are low pass filters that convert PWM voltage to a near sine-wave and eliminate both reflected voltage and (L-L) *dv/dt* concerns. In addition, sine-wave filters reduce ripple in the current waveform, typically reducing current distortion to less than 5 % THD-i.

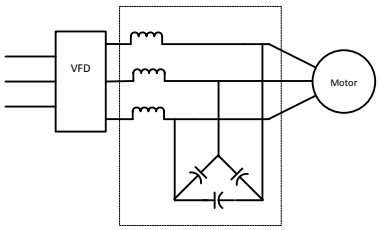

Fig. 13a Typical Sine-wave Filter

Computer simulation illustrates the typical motor voltage (Fig. 13b) and current (Fig. 13c) for a ASD with a sine-wave filter.

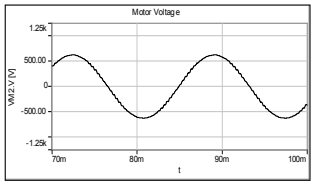

Fig. 13b Motor voltage

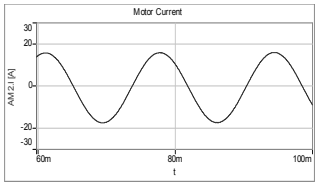

Fig. 13c Motor Current

Motor tests were performed using the 10 hp, 460 V ASD equipped with a sine-wave filter at the ASD output terminals. Inductance (L) is 4.8mH and the capacitors (C) are 4.7 µF each. Although the sine-wave filter is a differential mode filter, it also reduced the common-mode peak current, of which bearing currents are some percentage. Fig. 14 illustrates the measurements made for the ASD fed motor with a sine-wave filter. Bearing voltage is noticeably greater with the sine-wave filter than without it (Table VI). Therefore, the sine-wave filter alone cannot protect both the motor windings and bearings.

460V, 10 hp with Sine-wave Filter (5 *m*s)		
CH 1 (blue)	Motor current	8.247 A_{rms}
CH 2 (red)	C-M current	176.4 mA_{rms} / 1.11 A_{pk}
CH 3 (green)	Motor L-L voltage	695 V_{pk}
CH 4 (pink)	Shaft voltage	4.341 V_{rms} / 28.36 V_{pk}

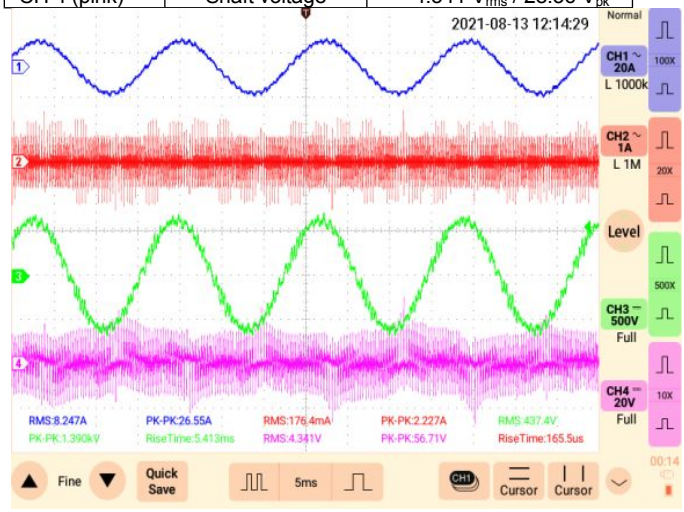

Fig. 14 (460V, 10 hp) Measurements with Sine-wave filter

Observations: the motor current waveform now has less high-frequency ripple than without the filter; the RMS value of the common-mode (C-M) current increased slightly (from 159.6 *m*A to 176.4 *m*A), but the peak C-M current reduced (from 1.90 A_{pk} to 1.11 A_{pk}). Motor bearing current will be some portion of the C-M current. L-L motor voltage was restored to a near sine-wave with about 5% distortion and the reflected pulses have been eliminated; motor shaft voltage increased from 16.2 V_{pk} to 28.36 V_{pk}, increasing the possibility of a bearing lubricant dielectric breakdown.

Table VI compares the critical values for the 460 V motor for two cases: (1) the motor alone (refer to Fig. 11) and (2) the motor with a sine-wave filter (refer to Fig. 14).

TABLE VI: 10 HP MOTOR COMPARISON: WITH AND WITHOUT SINE-WAVE FILTER

/20/$31.00 © 2022 IEEE

Sine wave filter	Motor Voltage (peak)	Shaft Voltage (peak)	Common Mode Current (RMS)	Common Mode Current (peak)
Yes	695 V_{pk}	28.36 V_{pk}	176.4 mA_{rms}	1.113 A_{pk}
No	1,109 V_{pk}	16.20 V_{pk}	159.6 mA_{rms}	1.905 A_{pk}

Analysis of the effects of the sine-wave filter on common-mode voltage (V_{sng}), C-M current and shaft voltage was also performed using the 5 hp, 230 V motor with the same 26 m cable. This test uses the 230 V motor operating at 30 Hz along with the previous filter. The measurements are tabulated here, and waveforms are shown further below in Fig. 15. Due to the operation at a lower voltage (230 V), V_{sng} and shaft voltage will naturally be lower by a factor of 2.

/20/$31.00 © 2022 IEEE

230 V, 5 hp with Sine-wave Filter (200 µs)		
CH 2 (red)	C-M current	102.1 mA_{rms} / 420 mA_{pk}
CH 3 (green)	V_{sng}	323 V_{pk}
CH 4 (pink)	Shaft voltage	5.059 V_{rms} / 11.92 V_{pk}

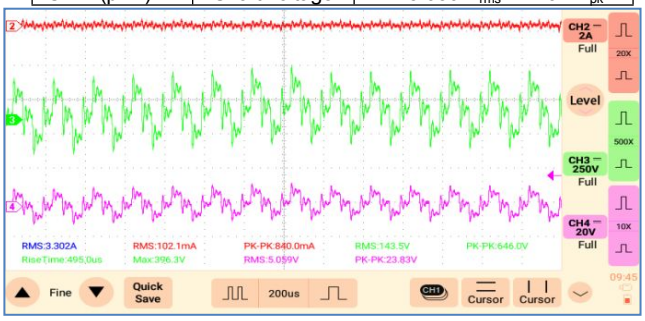

Fig. 15: 230 V, 5 hp V_{sng} and shaft voltage with sine-wave filter

Observations: V_{sng} is nearly double the expected value of 162.5 V_{pk} due to voltage reflection (cable length) plus oscillation resulting from the addition of filter inductance [5], [27]; shaft voltage (11.92 V_{pk}) increased above the baseline value (9.86 V_{pk}) due to voltage reflection and oscillation.

Table VII compares the critical values for the 5 hp, 230 V motor (26 m cable) for two cases: (1) the motor alone (Fig. 12) and (2) motor with sine-wave filter (Fig. 15).

TABLE VII: COMPARISON: WITH AND WITHOUT SINE-WAVE FILTER

Sine wave filter	V_{sng}	Shaft Voltage (peak)
Yes	323.0 V_{pk}	11.92 V_{pk}
No	266.6 V_{pk}	9.86 V_{pk}

Although the sine-wave filter restored sinusoidal (L-L) voltage for the motor, which has positive benefits, it resulted in higher V_{sng} and higher shaft voltage. Therefore, it is not a complete solution for both motor winding and bearing protection.

B. Sine-wave filter plus shaft grounding brush

Further testing was conducted using a sine-wave filter plus a shaft grounding brush. For this test, the 10 hp, 460 V motor was fitted with two low impedance (silver-graphite) shaft grounding brushes (Fig. 16). One is used to ground the shaft while the other measures shaft voltage.

Fig. 16 Motor with shaft grounding brush and shaft voltage measurement brush

A popular technique for bearing protection involves grounding of the motor shaft [3], [4], [5], [9], [14], [15], [18], [20], [21], [27], [32], [34]. This provides a low impedance path from the shaft to ground that shorts out the bearing capacitance and prevents voltage from building up on the motor shaft. The shaft grounding brush maintains equipotential for the shaft and frame [23].

Fig. 17 illustrates the measurements for the 460 V, 10 hp motor using both a sine-wave filter and shaft grounding brush. The oscilloscope was set at 5 *m*s/div for easy viewing of multiple cycles.

460 V, 10 hp Grounded Shaft + Sine-wave Filter (5 *m*sec)		
CH1 (blue)	Motor current	8.385 A_{rms}
CH 2 (red)	C-M current	174.8 *m*A / 1.08 A_{pk}
CH 3 (green)	Motor voltage (L-L)	695 V_{pk}
CH 4 (pink)	Shaft voltage	117.8 mV_{rms} / 822 mV_{pk}

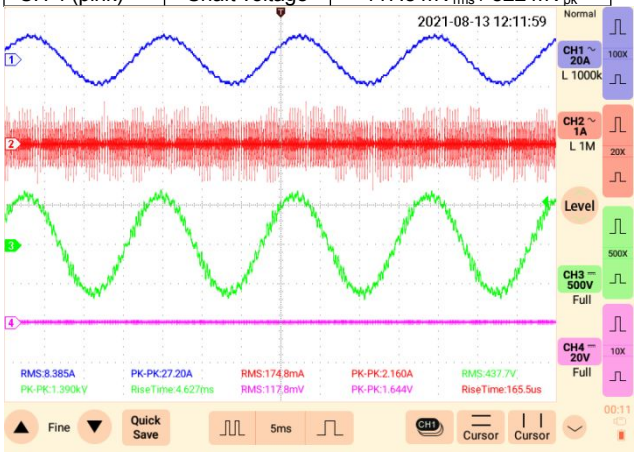

Fig. 17: 460 V, 10 hp motor at 5 *m*s time scale

Observations: Motor current is nearly sinusoidal with some ripple at f_{sw}; C-M peak current reduced to 1.08 Apk; RMS C-M current increased slightly; motor (L-L) voltage is nearly sinusoidal and without reflection; shaft voltage (822 mV_{pk}) is less than the EPRI [31] suggested limit (1 V_{rms} / 1.414 V_{pk}).

Table VIII compares values for the 460 V, 10 hp, 26 m cable motor for two cases: (1) the motor alone (Fig. 11) and (2) the motor with sine-wave filter plus shaft grounding brush (Fig. 17).

TABLE VIII: 10 HP MOTOR ALONE VS. SINE-WAVE FILTER PLUS GROUNDED SHAFT

Sine-wave Filter	Shaft Grounding Brush	Motor Voltage (peak)	Shaft Voltage (peak)	C-M Current (RMS)	C-M Current (peak)
No	No	1,109 V_{pk}	16.2 V_{pk}	159.6 mA_{rms}	1.90 A_{pk}
Yes	Yes	695 V_{pk}	0.82 V_{pk}	174.8 mA_{rms}	1.08 A_{pk}

Ideally, the motor peak voltage should be ≤1,000 V_{pk} with a rise time of 2 *u*sec or slower (NEMA std MG-1 [10], part 30) and shaft voltage should be less than 1.414 V_{pk} (EPRI) [31]. With the combination of sine-wave filter plus the shaft grounding brush, L-L voltage was sinusoidal and considerably lower than 1,000 V_{pk}, plus the rise time is substantially greater than 2 μs. Additionally, the shaft voltage is less than EPRI [31] suggested limit of 1.414 V_{pk}.

Common-mode voltage (V_{sng}) and shaft voltage were also analyzed for the combination of sine-wave filter and shaft grounding brush, using the 5hp, 230 V motor. At this lower voltage, V_{sng} and shaft voltage are expected to be a factor of two lower than the 460 V tests. Results are shown in Fig. 18.

/20/$31.00 © 2022 IEEE

Grounded Shaft and Sine-wave Filter (200 µs)		
CH 3 (green)	V_{sng}	348 V_{pk}
CH 4 (pink)	Shaft voltage	0.131 V_{rms} / 0.411 V_{pk}

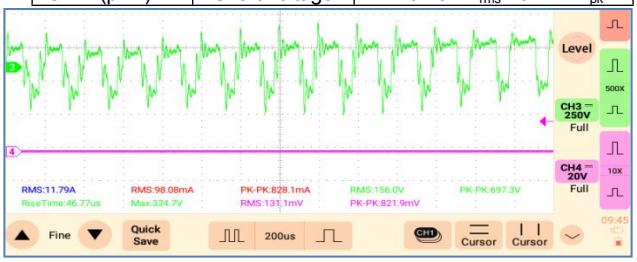

Fig. 18: 5 hp, 230 V motor at 200 µs/div

Observations: V_{sng} (348 V_{pk}) is higher than normal due to voltage reflection plus oscillation due to filter inductance; the shaft voltage is 0.411 V_{pk} which is less than the EPRI [31] suggested limit (1.414 V_{pk}).

Table IX compares the V_{sng} and shaft voltages for the 230 V, 5 hp motor for three cases: (1) the motor alone (Fig. 11), (2) the motor with sine-wave filter (Fig. 15), (3) the motor with the sine-wave filter plus shaft grounding brush (Fig. 18).

TABLE IX: 230 V, 5 HP MOTOR ALONE VS. SINE-WAVE FILTER WITH & WITHOUT SHAFT GROUNDING BRUSH

Sine-wave Filter	Shaft Grounding Brush	V_{sng}	Shaft Voltage (peak)
No	No	266.6 V_{pk}	9.86 V_{pk}
Yes	No	323.0 V_{pk}	11.92 V_{pk}
Yes	Yes	348.5 V_{pk}	0.411 V_{pk}

Table IX results illustrate the combination of sine-wave filter plus shaft grounding brush restored L-L voltage to a sine-wave and reduced shaft voltage to less than the EPRI [31] suggested limit. However, it demonstrates that the sine-wave filter alone does not mitigate shaft voltage. Therefore, comprehensive protection of motor windings and bearings requires the combination of a sine-wave filter plus a shaft grounding brush.

V. OTHER TECHNIQUES CONSIDERED

Other techniques have also been considered by several other authors and by us.

Soft Switching:

Soft-switching inverters reduce *dv/dt*, but do not reduce V_{sng} or shaft voltage any better than the typical (hard switching) inverter. The authors of [9], [30], [33] have stated that soft-switching inverters produce a shaft voltage comparable to that caused by hard switching inverters. Furthermore, these publications point out that the use of soft-switching inverter techniques does not alleviate bearing discharge (EDM) currents.

Three-level inverter control:

Three-level inverters switch only ½ of the DC bus voltage at a time; therefore, if voltage reflection occurs, the resulting peak voltage will theoretically be 1.5 times $V_{dc\text{-}bus}$ (instead of 2.0 times $V_{dc\text{-}bus}$). In cases where the pulse rise time is very fast and thus the previous transient has not fully decayed before the next pulse reaches the end of the cable, it is possible to experience peak voltage in the range of twice the DC bus voltage.

Fig. 19a illustrates the ASD output voltage for a 3-level inverter and Fig. 19b shows V_{sng} for the 3-level output.

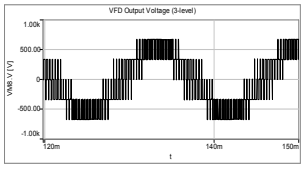

Fig. 19a L-L Voltage (3-level)

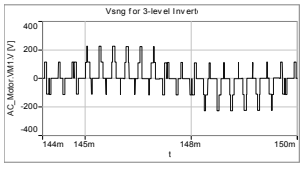

Fig. 19b V_{sng} (3-level)

For 3-level inverters, V_{sng} is typically one third $V_{dc\text{-}bus}$, which is about 225 V for a 480 V drive system. Where long motor cables are involved, voltage reflection will increase the L-L voltage, L-N voltage and V_{sng}. For example, Fig. 20a demonstrates the L-L motor voltage for a 460 V 3-level inverter with a long motor cable. Voltage reflection is visible, yet peak voltage is marginally below the 1,000 V_{pk} limit of NEMA MG-1 [10], pt 30.

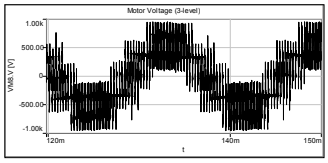

Fig. 20a (L-L) Voltage (3-level)

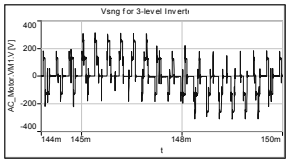

Fig. 20b V_{sng} (3-level))

Fig. 20b demonstrates that V_{sng}, responsible for bearing voltage, also increased due to voltage reflection associated with the cable. Since V_{sng} is increased, the potential for higher shaft voltage also increases.

The 3-level inverter technique reduces the common-mode voltage (V_{sng}) by switching only one-half of the DC bus voltage at a time, which generally results in reduced shaft voltage. Nevertheless, bearing discharge currents are still possible, especially in the case of voltage reflection due to motor cable length exceeding l_{cr}. For shorter cable lengths, 3-level inverters can offer favorable results; however, they may provide only marginal protection of motor windings and bearings where long motor cables are used. Additionally, since the waveform is still PWM, the motor still experiences higher losses than operation from pure sinusoidal voltage. Comprehensive motor protection, therefore, still requires a shaft grounding brush.

dv/dt Filters and Common Mode Chokes:

Article [21] indicates that "*dv/dt* filters and common-mode chokes do not reduce shaft voltage and the resultant EDM currents." Additionally, [34] states that *dv/dt* filters have no significant effects on bearing (discharge) currents. In addition, Muetze [20] points out that *dv/dt* filters are ineffective at reducing EDM currents, but methods that reduce common-mode voltage are effective.

Voltage waveforms (Fig. 21a-c) for a 230 V, 5 hp PWM drive with *dv/dt* filters were analyzed using computer simulation. The system had 26 meters of motor cable. DC bus voltage is 325 V; therefore, V_{sng} under normal conditions will be 162.5 Vpk.

/20/$31.00 © 2022 IEEE

Fig. 21a shows the ASD output voltage, while Fig. 21b shows the motor voltage when the *dv/dt* filter is used.

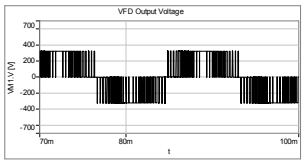

Fig. 21a ASD Voltage (L-L)

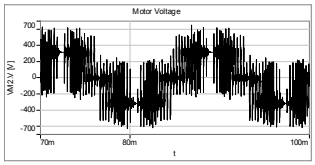

Fig. 21b Motor Voltage w/ *dv/dt* filter

The motor voltage waveform is still a PWM pattern and the peak voltage is nearly two times the DC bus voltage. Therefore, higher peak voltage can be expected for a longer cable. For example, in Fig. 21c, V_{sng} is over 300 V_{pk}; therefore, which is well above ½ DC bus voltage level and the shaft voltage will be higher than normal.

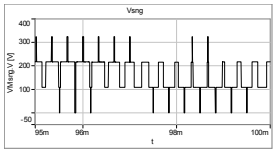

Fig. 21c V_{sng} with *dv/dt* filter

Computer simulation shows that the *dv/dt* filter does not reduce V_{sng} and therefore does not reduce shaft voltage, confirming the previous comments. Comprehensive motor protection, therefore, still requires shaft grounding.

VI. CONCLUSION

ASD controlled motors experience fast-rising pulses due to PWM voltage. Fast-rising PWM voltage pulses are responsible for *dv/dt*, voltage reflection and common-mode voltage (V_{sng}), which is the source of bearing voltage. Motors controlled by PWM drives can also experience higher operating temperatures than the same motor supplied from a sinusoidal voltage.

High *dv/dt* can stress motor insulation and lead to premature breakdown. It also causes voltage reflection, which increases motor peak voltage. Peak voltage becomes greater for longer cables. The sine-wave filter converted the voltage waveform to a sine-wave, slowed the rise time to the range of several milliseconds, similar to a motor operating on AC sine-wave voltage, reduced the *dv/dt* and eliminated the reflected voltage pulses. Simulation and test results confirm that this method can prevent excessive peak voltage due to reflection and reduce *dv/dt* to levels below the limits of NEMA MG-1, pt 31 and pt 30.

PWM drives cause common-mode voltage (V_{sng}), measured from stator neutral to frame ground. V_{sng} is the source of shaft (bearing) voltage. It distributes proportionately across the parasitic capacitances in the motor, resulting in a build-up of shaft voltage. When shaft voltage exceeds the dielectric withstand capability of the bearing lubricant, electrical discharge (EDM) currents can cause pitting or fluting of the bearing races.

ASD fed motor tests confirmed that the shaft grounding brush effectively shorted out the bearing capacitance and reduced the shaft voltage of the 460 V, 10 hp motor to less than 1 Volt ($_{pk}$), and the 230 V, 5 hp motor to less than 0.5 V_{pk}. which are below the EPRI suggested limit of 1.414 V_{pk}. Since shaft voltage is proportional to V_{sng} and DC bus voltage, then for a 575 V motor, it is expected that shaft voltage could be less than 1.25 V_{pk}. Bearing voltage is a function of the shaft grounding impedance. Although a single brush will protect most motor bearings, multiple brushes can be used in parallel either for large diameter shafts or to lower the shaft to ground impedance.

Computer simulation and confirmation testing demonstrated that the combination of sine-wave filter plus shaft grounding brush can effectively protect ASD fed motors. PWM-controlled motors will also operate with lower temperature rise when the PWM voltage is converted to a sine-wave. Neither method alone offers complete protection for the motor, however, the combination of sine-wave filter plus shaft grounding brush provides comprehensive protection for the windings and bearings while also reducing the motor operating temperature.

VII. REFERENCES

[1] US. Industrial and Commercial Motor System Market Assessment Report, Volume 2: Advanced Motors and Drives Supply Chain Review" September 2021. Energy Technologies Area, Lawrence Berkeley National Laboratory.

[2] T.F. Lowery, and D.W. Petro, "Applying PWM-Inverter Power To Low Voltage Induction Motors: Why Should Engineers Be Concerned?," Reliance Electric, Cleveland, OH, Conference Record of 1993 Forty-Fifth Annual Conference of Electrical Engineering Problems in the Rubber and Plastics Industries, April 1993, Page(s): pp 114 - 119.

[3] A. von Jouanne, H. Zhang, "A Dual Bridge Inverter Approach to Eliminating Common Mode Voltages and Bearing and Leakage Currents". IEEE Transactions on Power Electronics, Vol. 14, No. 1, January, 1999, pp 43-48.

[4] S. Chen, T. Lipo, D. Fitgerald, "Source of Induction Motor Bearing Currents Caused by PWM Inverters", UW-Madison, UW-Madison, Magnetek. IEEE Transactions on Energy Conversion, Vol. 11, No. 1, March, 1996, pp 25-32.

[5] S. Bell, R. Epperly, T. Cookson, A. Fischer, S. Cope, D. Schlegel, G. Skibinski, "Experience With Variable Frequency Drives and Motor Bearing Reliability". IEEE PCIC Conference, Paper, PCIC-98-27.

[6] I. Boldea, S.A. Nasar, "Electric Drives Third Edition" CRC Press, 2017.

[7] X. Ding,C. Chris Mi, "Impact of Inverter on Losses and Thermal Characteristics of Inductions Motors". Int'l Journal of Power Electronics, Vol. 3, No. 6, 2011, pp 641-651.

[8] MD. Texiera and J.A. Houdek, "Protecting Submersible Motors from the Effects of PWM Voltage", Brazil Conference for Quality of Electric Energy (CBQEE), 2009.

[9] D. Busse, J. Erdman, R. Kerkman, D. Schlegel and G. Skibinski, "Characteristics of Shaft Voltage and Bearing Currents", Rockwell Automation. IEEE Industry Applications Magazine, Nov/Dec 1997, pp 21-32.

[10] ANSI/NEMA standard MG-1-2016, Motors & Generators

[11] R.Kerkman, D. Leggate, G. Skibinski, "Interaction of Drive Modulations and Cables Parameters on AC Motor Transients", Rockwell Automation. IEEE Transactions on Industry Applications, Vol. 33, No. 3, May/June 1997, pp 722-731.

[12] L. Saunders, G. Skibinski, S. Evon, D. Kempkes, "Riding the Reflected Wave – IGBT Drive Technology Demands New Motor and Cable Considerations". IEEE PCIC Conference Paper, PCIC-96-09.

[13] E. Persson, "Transient Effects in Applications of PWM Inverters to Induction Motors". IEEE Transactions on Industry Applications, Vol. 28, No. 5, Sept/Oct 1992, pp 1095-1101.

/20/$31.00© 2022 IEEE

[14] Technical Specification IEC TS 60034-25:2014, Part 25: AC Electrical Machines Used in Power Drive Systems – Application Guide.
[15] NEMA Standards Publication ICS 7.2-2015, Application Guide for AC Adjustable Speed Drive Systems.
[16] R.F. Schiferl, M.J. Melfi, "Bearing Current Remediation Options".IEEE Industry Applications Magazine, July/Aug 2004, pp 40-50.
[17] S. Chen, T. Lipo, "Circulating Type Motor Bearing Current in Inverter Drives". IEEE Industry Applications Magazine, Jan/Feb 1998, pp 32-38.
[18] GAMBICA / BEAMA Technical Guide, Motor Shaft Voltages and Bearing Currents Under PWM Inverter Operation, March 2016.
[19] P. Link, "Minimizing Electric Bearing Currents in ASD Systems". IEEE Industry Applications Magazine, Jul/Aug 1999, pp 55-66.
[20] A. Muetze, "Bearing Currents in Inverter-Fed AC-Motors", Shaker Verlag, 2004.
[21] K. Vostrov, J. Pyrhonen, P. Linden, M.Niemela, J. Ahola, "Mitigation of Inverter-Induced Noncirculating Bearing Currents by Introducing Grounded Electrodes into Stator Slot Openings", IEEE Transactions on Industrial Electronics, Vol 68, No 12, Dec 2021, pp 11752-11760.

[22] D. Busse, J. Erdman, R. Kerkman, D. Schlegel, G. Skibinski, "Bearing Currents and Their Relationship to PWM Drives", IEEE Transactions on Power Electronics, Vol. 12, No. 2, March, 1997, pp 243-252.
[23] J. Erdman, R. Kerkman,D. Schlegel, G. Skibinski, "Effect of PWM Inverters on AC Motor Bearing Currents and Shaft Voltages", IEEE APEC Conference, Dallas, March 1995.
[24] M. Aqil, J. Im, J. Hur, "Application of Perovskite Layer to Rotor for Enhanced Stator-Rotor Capacitance for PMSM Shaft Voltage Reduction", Energies 2020, 13, 5762.
[25] D. Busse, J. Erdman, R. Kerkman, D. Schlegel, G. Skibinski, "The Effects pf PWM Voltage Source Inverters on the Mechanical Performance of Rolling Bearings", IEEE Transactions on Industry Applications, Vol. 33, No. 2, Mar/Apr 1999, pp 567-576.
[26] R. Riehl, F. de Souza Campos, A. Alves, E. Filho, "Analysis and Methodology for Determining the Parasitic Capacitances in VSI-Fed IM Drives Based on PWM Technique", INTECH, Chapter 3, 2015
[27] D. Macdonald, W. Gray, "PWM Drive Related Bearing Failures", IEEE Industry Applications Magazine, Jul/ Aug, 1999, pp41-47.
[28] N. Bader, A. Furtmann, H. Tischmacher, G. Poll. "Capacitances and Lubricant Film Thicknesses of Grease and Oil Lubricated Bearings", Society of Tribologists and Lubrication Engineers Annual Meeting Conference Paper. STLE Atlanta, May 21-25, 2017.
[29] D. Busse, J. Erdman, R. Kerkman, D. Schlegel, G. Skibinski, "System Electrical Parameters and Their Effects on Bearing Currents", IEEE Transactions on Industry Applications, Vol. 33, No. 2, Mar/Apr 1997, pp 577-584.
[30] S. Bhattacharya, L. Resta, D. Divan, D. Novotny, "Experimental Comparison of Motor Bearing Currents with PWM Hard- and Soft-Switched Voltage-Source Inverters", IEEE Transactions on Power Electronics, Vol 14, No. 3, 1999, pp 552-562.
[31] EPRI PQ News, October 2007, "The Effects of Shaft Voltage and Bearing Current on Motors driven by Variable Frequency Drives"
[32] J.D. Koenitzer, P.E., "Shaft Grounding and Sliding Electrical Contacts". Helwig Carbon Products, 2016.
[33] S. Chen, T. Lipo, "Bearing Currents and Shaft Voltages of an Induction Motor Under Hard- and Soft-Switching Inverter Excitation", IEEE Transactions on Industry Applications, Vol. 34, No. 5, Sept/Oct 1998, pp1042-1048.
[34] A. von Jouanne, H. Zhang, A. Wallace "An Evaluation of Mitigation Techniques for Bearing Currents, EMI and Overvoltages in ASD Applications", IEEE Transactions on Industry Applications, Vol. 34, No. 5, Sept/Oct, 1998, pp 1113-1122.

VIII. VITAE

John Houdek (IEEE Life Senior Member) graduated (1981) from the Milwaukee School of Engineering (MSOE), with a Bachelor's Degree in Electrical Engineering Technology, and from Keller Graduate of Management (1989) with a Master's Degree in Business Administration (MBA). His prior employment experience included Square D Company, Eaton Cutler Hammer, Trans-Coil, Inc., and MTE Corporation. Houdek presently serves as a power quality consultant at Allied Industrial Marketing, Inc. of which he has been a co-owner since 2003. His special field of interest is in power quality related areas including inverter power quality and motor power factor. Houdek has authored many technical papers on various aspects of electrical power quality and has delivered power quality seminars throughout the world. For twenty years, Houdek taught power quality courses at MSOE.

Nitin Kulkarni graduated (BSME 1995) from the Shivaji University, India with a Bachelor's Degree in Mechanical Engineering, completed Master's Degree in Mechanical Engineering from Tuskegee University, Alabama (MSME 2002) and Executive Master's Degree in Business Administration (EMBA 2010) from Marquette University, Wisconsin. His employment experience included Godrej-Lawkim Motors, and Specialty Motors. Kulkarni presently serves as Vice President of Engineering and Business Development at Helwig Carbon Products Inc. His special field of interest is improving life and performance of Electrical Motors and equipment. His research is focused on Electro-Mechanical Engineering and Material Science for sliding electrical contact. Kulkarni has presented and authored many technical papers on various aspects of electrical motors and material science. For last twenty-five years, Kulkarni is contributing to Electrical Motors Industry. He also serves on Technical Committee of The Electrical Apparatus Service Association, Inc. (EASA), an international organization.

Randy Herche is R&D Manager at Helwig Carbon Products works with customers, sales reps, and operations to produce new carbon brush grades. Randy has experience in developing carbon brush materials for specific applications, such as special grades for shaft grounding. Randy also has extensive experience in testing carbon brushes and the processing of the material to achieve the desired results. Randy has a BS in Chemical Engineering from the University of Wisconsin, and over thirty years at Helwig Carbon Products. Randy currently lives in Oconomowoc Wisconsin enjoying family, gardening, and woodworking.

/20/$31.00© 2022 IEEE